Focal averaging and incoherent scattering in laser-assisted radiative recombination and scattering processes

A. Čerkić[1] and D. B. Milošević[2,3]
[1]*Federal Meteorological Institute, Bardakčije 12, 71000 Sarajevo, Bosnia and Herzegovina*
[2]*Faculty of Science, University of Sarajevo, Zmaja od Bosne 35, 71000 Sarajevo, Bosnia and Herzegovina*
[3]*Max-Born-Institut, Max-Born-Strasse 2a, 12489 Berlin, Germany*
(Received 13 September 2006; published 16 January 2007)

Two different strong-laser-field-assisted atomic processes are considered: the laser-assisted electron-ion radiative recombination (LAR) and the laser-assisted electron-atom scattering (LAS). Assuming Gaussian space-time distribution of laser intensity in focus, we calculated the focal-averaged spectra for these processes. These spectra form plateaulike structures and are qualitatively similar to the spectra calculated for fixed intensity. The difference is that for the focal-averaged results, the plateaus are more inclined and the oscillatory structures are suppressed (or even absent). We also investigate the contribution of incoherent electron scattering off neighboring atoms (ions) to the LAR and LAS spectra. We suppose that an electron, after the scattering on an ionic target, may recombine with another ion (we call this process ISLAR—incoherent scattering followed by LAR). Analogously, the electron that scatters on an atom in the LAS process may scatter once more on another atom (this is the double scattering). In both cases, two targets are involved and the process is incoherent. The spectra that involve these incoherent processes are compared with the corresponding spectra for the coherent LAR and LAS processes, in which an additional act of scattering off the same target is included. If the density of atomic targets is high enough, the contribution of incoherent scattering can be larger than the contribution of coherent scattering. The spectra of ISLAR and double scattering exhibit a cutoff-like behavior, having much higher cutoff energies than that of LAR and LAS.

DOI: 10.1103/PhysRevA.75.013412 PACS number(s): 34.80.Qb, 34.80.Lx, 32.30.Rj, 34.50.Rk

I. INTRODUCTION

With the development of powerful laser systems, the intense-laser–atom physics has entered the nonperturbative regime. Generally, the atomic processes that take place in strong laser fields can be categorized into two main groups: laser-assisted processes and laser-induced processes [1]. The laser-assisted processes can happen in the absence of the laser field and they are only modified by the simultaneous interaction with laser radiation. This modification can be strong since very many photons can be absorbed from the laser field. For example, in the laser-assisted electron-ion radiative recombination (LAR) [2–9], laser-assisted electron-atom scattering (LAS) [10–13], and laser-assisted x-ray-atom scattering [14,15], the emitted photon and electron spectra exhibit a long plateau, formed due to absorption of a large number of laser photons, followed by an abrupt cutoff. The position of this cutoff was explained semiclassically, supposing that, in one phase of the process, the quantum-mechanical interaction of the electron with the atom (or ion) can be neglected in comparison with the electron-laser-field interaction (which can be treated classically) (see, for example, Ref. [16], where all these processes were considered on a common base). Even multiplateau structures in such processes were predicted (see Refs. [4] for LAR, [11,12] for LAS, and [15] for x-ray-atom scattering). It should be mentioned that the LAR process in the presence of an ultrashort few-cycle laser pulse has recently attracted more attention [8,9].

The laser-induced processes can happen only in the presence of a laser field and they usually require a threshold value of the number of absorbed laser photons. For example, for above-threshold ionization (ATI), the minimum number N of photons necessary for ionization is at the same time the lowest order of nonlinearity of this process. The ATI electron spectra exhibit peaks at electron energies [17] $E_p=n\omega-|E_B|-U_P$, where E_B is the electron binding energy and $U_P=I/(4\omega^2)$ is the ponderomotive energy of the free electron in the laser field. These peaks, separated by the photon energy ω, for a fixed laser-field intensity I, correspond to the absorption of $n=N,N+1,N+2,\ldots$ laser photons. With the increase of the laser intensity, N photons are no longer sufficient and $N+1$ photons are necessary for ionization. One says that the N-photon channel is closed [18]. This channel-closing effect has important consequences for the behavior of ATI spectra as a function of the laser-field intensity: at some particular value of intensity, the ionization yield exhibits a resonant behavior. These enhancements in high-order ATI spectra at the channel-closing intensities were observed experimentally (see references in [19]). Due to the spatio-temporal intensity distribution in the laser focus, the atoms feel the laser field whose intensity changes from $I=0$ to $I=I_{\max}$. The corresponding channel-closing intensities are $I_c=(N_c\omega-|E_B|)4\omega^2$, $N_c=N_{c,\min},N_{c,\min}+1,\ldots,N_{c,\max}$, where $N_{c,\min}=[|E_B|/\omega]+1$ and $I_c\leqslant I_{\max}$. For these intensities, we have enhancements in the electron spectra. Therefore, for a comparison with the experiment, the theoretical energy spectrum of the ionized electrons, which was calculated for a fixed intensity, has to be integrated over the intensity distribution in the laser focus.

The laser-assisted processes can happen in the absence of the laser field, so that for these processes there are no channel-closing effects and enhancements of the particular spectral regions for $N>0$. Nevertheless, it will be interesting to see how these spectra change if one performs the focal

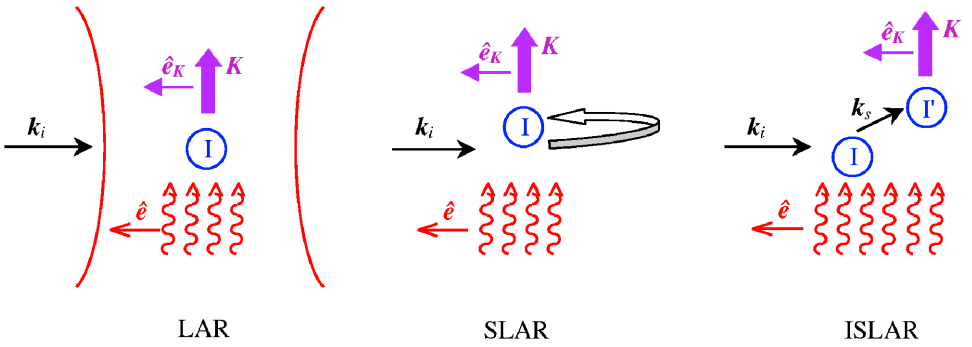

FIG. 1. (Color online) Schematic diagram of the laser-assisted radiative recombination (LAR) (left-hand part; laser beam in the focal region is also denoted), LAR with rescattering (middle part, SLAR), and LAR preceded by incoherent scattering (right-hand part, ISLAR).

averaging. For low-order electron-atom scattering, attempts to simulate scattering experiments were done in Refs. [20,21] in the context of the experiments of Weingartshofer *et al.* [22]. However, the influence of the focal averaging on the plateau structures has never been analyzed [23]. The focal-averaging method, developed in Ref. [24] in order to simulate high-order ATI experiments, is more appropriate for spatio-temporal intensity distribution of the laser fields generated by modern laser systems. One of the aims of the present paper is to investigate the focal-averaging effects on the laser-assisted processes. We will do this using the examples of high-order LAR and LAS processes.

If the density of the atomic or ionic beam used in a laser-assisted experiment is high, then it is possible that the electron first scatters on an atomic (ionic) target and, after that, the scattered electron takes part in the considered laser-assisted process. For example, in the LAR process, the incoming electron may first scatter on an ion I and then recombine with a different ion I', emitting an x-ray photon. We have already analyzed in Ref. [4] the LAR process in which the electron was first scattered on an ion and then was recombined with the same ion. We have denoted this process SLAR. Here "S" stands for coherent scattering since the amplitude of the direct LAR process and that of the LAR process preceded by a scattering off the same ion add coherently. However, if the electron first scatters on an ion and then recombines with a different ion, then the amplitude of this process and that of the direct LAR process add incoherently, i.e., we sum the probabilities of these processes. Therefore, we call the LAR process preceded by an incoherent scattering (IS) of an incoming electron on a different ion the ISLAR process. All these processes are schematically presented in Fig. 1 [25]. We will show in the present paper that the emitted x-ray spectra of ISLAR look quite different from the LAR spectra.

A similar consideration can be made for the LAS process. The LAS preceded by scattering on a different atom was named double scattering in Refs. [26,27], where this process was proposed in order to explain a discrepancy between the Kroll-Watson theory of electron-atom scattering [28,29] and the LAS experiments for particular values of the scattering angle [30]. In the present paper, we will analyze the double scattering in more detail and we will compare it with the results for the LAS process preceded by the coherent scattering, which leads to the appearance of an additional plateau in the electron spectrum [11,12]. The schematic picture of the LAS process will be similar to that of LAR, presented in Fig. 1. The only difference is that the incident electron momentum $\boldsymbol{k}_i$ is parallel to the laser-field polarization vector $\hat{\boldsymbol{e}}$ and that, in the final state, the x-ray photon $\boldsymbol{K}$ is replaced with the outgoing electron having the momentum $\boldsymbol{k}_f$.

It should be mentioned that, besides the electron-atom scattering experiments by Weingartshofer *et al.* [22,31], which were continued by Wallbank and Holmes [23,30], there exist other laser-assisted experiments. Mason and Newell [32] have observed simultaneous electron-photon excitation of He in inelastic laser-assisted electron-atom collisions. More recently, the laser-assisted electron impact ionization was experimentally observed [33]. In these experiments, the laser intensity was lower and the laser pulse duration was longer than for the processes that we will consider in the present paper.

The structure of our paper is the following. In Sec. II, we will briefly describe our focal-averaging procedure. Then, in Sec. III, we will present the theory of the ISLAR process. In particular, in Sec. III B, we will derive the cutoff law for this process. A similar analysis of the double-scattering process is presented in Sec. IV. Section V contains our numerical results for the focal-averaged LAR and LAS spectra, while the numerical results for incoherent processes are presented in Sec. VI. Finally, Section VII contains our conclusions.

II. THE METHOD OF FOCAL AVERAGING

In this paper, we present the focal-averaged spectra for the LAR and LAS processes. The focal averaging is done by integrating over the spatio-temporal intensity distribution in the laser focus. We assume a Gaussian spatio-temporal distribution of the laser intensity

$$I(r,z,t) = \frac{I_{\max}}{1+z^2/z_0^2} \exp\left[-\frac{2r^2}{w_0^2(1+z^2/z_0^2)} - \frac{(t-z/c)^2 4\ln 2}{\tau_p^2}\right], \tag{1}$$

where r and z are circular-polar coordinates with the z axis along the laser beam propagation direction, $I_{\max}$ is the maximum or peak intensity, w_0 is the beam waist (beam radius at $z=0$), z_0 is the Rayleigh range, and τ_p is the pulse duration time [full width at half maximum (FWHM)]. In the weak-focusing approximation [24], which we will use in all calculations in our paper, we neglect the dependence on z and choose $z=0$ in Eq. (1). In this case, the diameter of the target beam is small compared with the Rayleigh range of the laser beam focus. The derivation similar to that presented in Ref.

[24] leads to the following expression for the focal-averaged x-ray photon yield of LAR process:

$$\langle S_{fi}\rangle \propto \int_0^{I_{\max}} \frac{dI}{I}\left(\ln\frac{I_{\max}}{I}\right)^{1/2}\sum_n S_{fi}(n) \times \delta(\omega_K - E_i - |E_B| - n\omega - I/(4\omega^2)). \quad (2)$$

Here I is the laser-field intensity, which changes from zero to a maximum value $I_{\max}$, ω_K is the energy of the emitted x-ray photon, E_i is the incident electron kinetic energy, E_B is the atomic binding energy, and $S_{fi}(n)$ is the differential power spectrum for emission of an x-ray photon [1,4]. The δ function cancels the integral over I so that, for every ω_K, $\langle S_{fi}\rangle$ can be calculated as a single sum over n, with $n\omega \geqslant \omega_K - E_i - |E_B| - I_{\max}/(4\omega^2)$ and $n\omega \leqslant \omega_K - E_i - |E_B|$.

Analogously, for the focal-averaged electron yield in the laser-assisted electron-atom scattering process, we obtain

$$\langle d\sigma_{fi}\rangle \propto \int_0^{I_{\max}} \frac{dI}{I}\left(\ln\frac{I_{\max}}{I}\right)^{1/2} d\sigma_{fi}, \quad (3)$$

where $d\sigma_{fi}$ is the differential cross section for the electron-atom scattering in the presence of the laser field having the intensity I [10,12]. The integral over I can be performed by numerical integration.

The factor of proportionality for the focal-averaged yield of the ATI process was found in Ref. [24]. Similarly as in this paper, we obtain that the yields in Eqs. (2) and (3) are proportional to the pulse length τ_p, the diameter d of the ionic (atomic) beam, and the square of the laser beam waist w_0.

III. ELECTRON-ION RADIATIVE RECOMBINATION PRECEDED BY INCOHERENT SCATTERING

A. Theory

We will first analyze the role of incoherent scattering in laser-assisted electron-ion radiative recombination. In the ISLAR process, the electron scatters on a positive ion and subsequently recombines with another ion. The entire process occurs in a laser field, for which we assume that it is linearly polarized with the electric field vector

$$\boldsymbol{E}(t) = \hat{\mathbf{e}}E_0 \sin\omega t, \quad (4)$$

intensity $I=E_0^2$, and angular frequency ω. The final result is the emission of an x-ray photon having wave vector $\boldsymbol{K}$, frequency (energy) ω_K, and unit polarization vector $\hat{\mathbf{e}}_K$. We use spherical coordinates with the polar axis in the direction of the polarization vector $\hat{\mathbf{e}}$ of the laser field. We also assume that the polarization vector $\hat{\mathbf{e}}_K$ of the x-ray field is parallel, while the incident electron momentum $\boldsymbol{k}_i$ is antiparallel to $\hat{\mathbf{e}}$. We have chosen this configuration since it provides the most favorable conditions for the generation of x rays [2]. Thus, we have $\hat{\mathbf{e}}=\hat{\mathbf{e}}_K=-\hat{\boldsymbol{k}}_i$ (see Fig. 1). The probability of the ISLAR process is proportional to the density $\mathcal{N}$ of the ionic beam and to its diameter (the thickness of the ionic target) d, i.e., it is proportional to the parameter $\rho=\mathcal{N}d$, which we will express in atomic units. In general, we suppose that the density of the ionic (atomic) beam in the interaction region is such that only the single scattering of electrons on the ions (atoms) is possible, while the multiple scattering [34] can be neglected.

The differential power spectrum for emission of an x-ray photon in the ISLAR process is given by the formula

$$S_{fi}^{\mathrm{IS}}(M) = \rho\sum_L \int_0^{2\pi} d\phi_s \int_0^{\pi} d\theta_s \sin\theta_s d\sigma_{si}(L,\Omega_s) S_{fs}(N,\Omega_s), \quad (5)$$

where L and N are the numbers of absorbed (emitted) photons in the electron-ion scattering and LAR process, respectively, $M=N+L$ is the total number of absorbed (for $M>0$) or emitted (for $M<0$) photons, $d\sigma_{si}(L,\Omega_s)$ is the differential cross section for electron-ion potential scattering, $S_{fs}(N,\Omega_s)$ is the differential power spectrum for LAR, the solid angle $\Omega_s \equiv (\theta_s,\phi_s)$ determines the direction of the electron momentum $\boldsymbol{k}_s$ after the scattering, and the sum over L involves all open channels for the scattering process. The electron energies before and after the scattering are E_i and E_s, respectively. Due to the energy-conserving condition for electron scattering, $E_s=E_i+L\omega$, a channel is open if $L>-E_i/\omega$. According to Eq. (5), the electron with the initial momentum $\boldsymbol{k}_i$ scatters on a positive ion in the laser field (4) and, having the momentum $\boldsymbol{k}_s$ after the scattering, subsequently recombines with another ionic target, producing an x-ray photon with the wave vector $\boldsymbol{K}$.

The differential power spectrum for the LAR process is [1]

$$S_{fs}(N,\Omega_s) = \frac{k_s\omega_K^4}{2\pi c^3}|T_{fs}(N,\Omega_s)|^2, \quad (6)$$

where the T-matrix element is given by

$$T_{fs}(N,\Omega_s) = \int_0^T \frac{dt}{T}\mathcal{T}_{fs}(t,\Omega_s)\exp(iN\omega t), \quad (7)$$

with $T=2\pi/\omega$ the laser-field period. The Fourier transform of the T matrix on the right-hand side of Eq. (7) is defined by

$$\mathcal{T}_{fs}(t,\Omega_s) = \exp\{-i[\boldsymbol{k}_s\cdot\boldsymbol{\alpha}(t)+\mathcal{U}_1(t)]\}\langle\psi_B|\boldsymbol{r}\cdot\hat{\mathbf{e}}_K e^{-i\boldsymbol{K}\cdot\boldsymbol{r}}|\boldsymbol{q}\rangle, \quad (8)$$

where $\boldsymbol{k}_s$ is the momentum of the recombining electron, $\boldsymbol{\alpha}(t)=\int^t dt'\boldsymbol{A}(t')$, $\boldsymbol{A}(t)=-\int^t dt'\boldsymbol{E}(t')$, ψ_B is the wave function of the atomic ground state, $\boldsymbol{q}=\boldsymbol{k}_s+\boldsymbol{A}(t)$, and $\mathcal{U}_1(t)$ is defined as the periodic part of $\mathcal{U}(t)=\frac{1}{2}\int^t dt'\boldsymbol{A}^2(t')=\mathcal{U}_1(t)+U_P t$, with U_P the ponderomotive energy. The T matrix (8) can also be written in the form

$$\mathcal{T}_{fs}(t,\Omega_s) = -i\exp\{-i[\boldsymbol{k}_s\cdot\boldsymbol{\alpha}(t)+\mathcal{U}_1(t)]\}\hat{\mathbf{e}}_K\cdot\frac{\partial}{\partial\boldsymbol{Q}}\tilde{\psi}_B(\boldsymbol{Q}), \quad (9)$$

with $\boldsymbol{Q}=\boldsymbol{k}_s+\boldsymbol{A}(t)-\boldsymbol{K}$, and

$$\tilde{\psi}_B(\boldsymbol{Q}) = \int \frac{d^3\boldsymbol{r}}{(2\pi)^{3/2}} \psi_B^*(\boldsymbol{r}) \exp(i\boldsymbol{Q}\cdot\boldsymbol{r}). \tag{10}$$

We calculate the integral in Eq. (7) numerically.

The differential cross section in Eq. (5) describes the potential scattering of an electron with initial momentum $\boldsymbol{k}_i$ on a local potential $V(\boldsymbol{r})$, so that the electron momentum after the scattering is $\boldsymbol{k}_s$ and that L photons are exchanged with the laser field. Within the first Born approximation, it is given by [35]

$$d\sigma_{si}(L,\Omega_s) = (2\pi)^4 \frac{k_s}{k_i} J_L^2(x) |V_{\boldsymbol{k}_i-\boldsymbol{k}_s}|^2, \tag{11}$$

where $J_L(x)$ is the ordinary Bessel function of order L, $x=(A_0/\omega)\hat{\mathbf{e}}\cdot(\boldsymbol{k}_i-\boldsymbol{k}_s)$, $A_0=E_0/\omega$, and $V_{\boldsymbol{k}_i-\boldsymbol{k}_s}$ is the Fourier transform of the scattering potential $V(\boldsymbol{r})$, defined by the formula

$$V_{\boldsymbol{P}} = \int \frac{d^3\boldsymbol{r}}{(2\pi)^3} V(\boldsymbol{r}) \exp(i\boldsymbol{P}\cdot\boldsymbol{r}). \tag{12}$$

There are also various more sophisticated theories of laser-assisted potential scattering such as the Kroll-Watson soft-photon approximation [28], the off-shell low-frequency approximation (impulse approximation) [36], R-matrix Floquet theory [37], the [1,1] Padé approximant to the Born series [29], and the eikonal approximation [38], but they will not affect the qualitative estimate of the effects of interest in the present paper.

We model the scattering potential by [39,40]

$$V(r) = -\left(a + \frac{b}{r}\right)\exp(-\lambda r), \tag{13}$$

whose Fourier transform is

$$V_{\boldsymbol{k}_i-\boldsymbol{k}_s} = -\frac{2b\lambda + aC}{2\pi^2 C^2}, \quad C = (\boldsymbol{k}_i-\boldsymbol{k}_s)^2 + \lambda^2. \tag{14}$$

In our paper, we will present the results for the He^+ ion ($a=1$, $b=2$, $\lambda=4$).

For our linearly polarized laser field (4) with the polarization vector in the direction of the polar axis and for the incident electron momentum $\boldsymbol{k}_i$ antiparallel to the polar axis, the T-matrix element, given by Eqs. (7)–(10), the Bessel function $J_L(x)$ in Eq. (11), and the Fourier transform of the scattering potential (14) are independent of the angle ϕ_s. As a consequence, the differential power spectrum S_{fs}, Eq. (6), and differential cross section $d\sigma_{si}$, Eq. (11), are independent of the polar angle ϕ_s.

Inserting Eqs. (6) and (11) into Eq. (5), and performing integration over the polar angle ϕ_s, we obtain

$$S_{fi}^{\mathrm{IS}}(M) = \rho \frac{(2\pi\omega_{\boldsymbol{K}})^4}{k_i c^3} \sum_L k_s^2 \int_0^\pi d\theta_s \sin\theta_s J_L^2(x) \times |V_{\boldsymbol{k}_i-\boldsymbol{k}_s}|^2 |T_{fs}(N,\theta_s)|^2. \tag{15}$$

The incident electron momentum $\boldsymbol{k}_i$ is chosen to be antiparallel to the polar axis, i.e., $\theta_i=\pi$. Therefore, S_{fi}^{IS} is independent of the azimuthal angle ϕ_i of electron incidence and the integration over ϕ_i is straightforward, leading to $2\pi S_{fi}^{\mathrm{IS}}$. This quantity will be presented in our numerical results.

Equation (5) describes two incoherent processes, with two energy-conserving conditions. The energy-conserving condition for the scattering process is $E_s=E_i+L\omega$, where $E_i=k_i^2/2$ is the incident electron energy and $E_s=k_s^2/2$ is the electron energy after the scattering. The direct LAR process provides the energy-conserving condition $\omega_{\boldsymbol{K}}=E_s+|E_B|+U_P+N\omega$, where E_B is the binding energy of the ion. Combining these two conditions, we have $\omega_{\boldsymbol{K}}=E_i+|E_B|+U_P+M\omega$, with $M=N+L$ the total number of absorbed (emitted) laser photons.

B. Cutoff law

The differential cross section for scattering of electrons on atomic (ionic) targets, presented as a function of the final electron energy, forms a plateau structure with an abrupt cutoff at some boundary value of energy, usually called the cutoff energy [12]. The same is true for the differential power spectrum of the LAR process, if we present it as a function of the x-ray photon energy [1]. Therefore, it is reasonable to suppose that the differential power spectrum of the ISLAR process has a cutoff at some boundary value of the x-ray photon energy. We will now estimate this energy. In the case of direct LAS, the method of steepest descent (stationary phase method) gives the semiclassical equation [12]

$$[\boldsymbol{k}_i + \boldsymbol{A}(t)]^2 = [\boldsymbol{k}_s + \boldsymbol{A}(t)]^2, \tag{16}$$

with $\boldsymbol{k}_i$ and $\boldsymbol{k}_s$ the electron momenta before and after the scattering, respectively, and t the scattering time. Equation (16), for the electric field (4) in the direction of the polar axis and with the incident electron momentum in the opposite direction ($\hat{\mathbf{e}}=-\boldsymbol{k}_i$), gives a quadratic equation for k_s, the solution of which is

$$k_s = -h \pm \sqrt{h^2 + k_i^2 - 2s}, \quad h = A_0 \cos\omega t \cos\theta_s,$$
$$s = k_i A_0 \cos\omega t. \tag{17}$$

One can see from the first of Eqs. (17) that the solution with the plus sign in front of the square root gives a higher value of k_s than the one with the minus sign. Our goal is to find the maximum energy of the scattered electron and thus we discard the solution with the minus sign. From the energy-conserving condition for electron scattering, we have

$$L\omega = \frac{1}{2}(k_s^2 - k_i^2) = h^2 - s - h\sqrt{h^2 + k_i^2 - 2s}. \tag{18}$$

In order to find $L_{\max}$ with respect to t and θ_s, we use the conditions $\partial(L\omega)/\partial t=0$ and $\partial(L\omega)/\partial\theta_s=0$ in Eq. (18). In this way, we obtain the conditions $\sin\omega t=0$ and $\sin\theta_s=0$, so that $\omega t=m\pi$ (with m integer) and $\theta_s=0,\pi$. This means that $\cos\omega t=\pm 1$ and $\cos\theta_s=\pm 1$, which implies that we have four solutions. From Eqs. (16)–(18) one can see that the maximum value of L is obtained for $\cos\omega t=-1$ and $\theta_s=0$, so that

$$L_{\max}\omega = 2(A_0^2 + k_i A_0) = 8U_P + 4\sqrt{2E_i U_P}. \tag{19}$$

Thus, the maximum electron energy after the scattering and before the recombination is $E_{s,\max}=E_i+L_{\max}\omega$, with $L_{\max}$

given by Eq. (19). It is well known that the maximum energy of the emitted x rays in the LAR process is [1]

$$\omega_{\boldsymbol{K},\max} = E_p + 2U_P + |E_B| + 2\sqrt{2E_pU_P}, \tag{20}$$

where E_p is the incident electron energy. Since in our case $E_p = E_{s,\max}$, we finally have

$$\omega^{\mathrm{IS}}_{\boldsymbol{K},\max} = 2U_P[(\gamma_i + 3)^2 + \gamma^2], \tag{21}$$

where $\gamma = \sqrt{|E_B|/(2U_P)}$ is the Keldysh parameter [41] and $\gamma_i = \sqrt{E_i/(2U_P)} = k_i/A_0$ is an analogous parameter that was introduced in Ref. [12]. For $U_P \gg \max\{E_i, |E_B|\}$, we have $\omega^{\mathrm{IS}}_{\boldsymbol{K},\max} \approx 18U_P$.

IV. DOUBLE SCATTERING

A. Theory

In the double electron-atom scattering, the electron with the incident momentum $\boldsymbol{k}_i$ scatters on an atomic target, proceeds to another atom, scatters on it, and leaves this atom having the final momentum $\boldsymbol{k}_f$. This process is incoherent. In Sec. VI, we will compare the double-scattering electron spectra with those for a coherent process, known as rescattering. In the rescattering process, the electron first scatters on the target, then leaves it driven by the laser field and returns to the target after the field has changed the sign, and finally scatters again on the same target.

In our analysis, we assume that the laser field is linearly polarized with the electric-field vector given by Eq. (4). We use spherical coordinates with the polarization vector $\hat{\mathbf{e}}$ of the laser field and the incident electron momentum $\boldsymbol{k}_i$ in the direction of the polar axis. The differential cross section for double scattering is defined by [26,27]

$$d\sigma^{\mathrm{DS}}_{fi}(M,\Omega_f) = \rho \sum_L \int_0^{2\pi} d\phi_s \int_0^{\pi} d\theta_s \sin\theta_s d\sigma_{si}(L,\Omega_s) \times d\sigma_{fs}(N,\Omega_s,\Omega_f), \tag{22}$$

where L and N are the numbers of absorbed (emitted) photons in the first and the second scattering, respectively, $M = N+L$ is the total number of absorbed (emitted) photons, $d\sigma_{si}(L,\Omega_s)$ and $d\sigma_{fs}(N,\Omega_s,\Omega_f)$ are the differential cross sections for the first and the second scattering, respectively, the solid angles $\Omega_s \equiv (\theta_s, \phi_s)$ and $\Omega_f \equiv (\theta_f, \phi_f)$ determine the directions of the electron momentum vector after the first and after the second scattering, respectively, and the sum over L involves all open channels for the scattering process $(L > -E_i/\omega)$. The constant ρ in Eq. (22) depends on the density $\mathcal{N}$ of atomic targets and on the thickness d of the target, i.e., $\rho = \mathcal{N}d$. According to Eq. (22), the electron with the initial momentum $\boldsymbol{k}_i$ scatters on a target in the laser field and, having the momentum $\boldsymbol{k}_s$ after the scattering, subsequently scatters on another target having the final momentum $\boldsymbol{k}_f$ after the second scattering.

The differential cross section $d\sigma_{si}(L,\Omega_s)$ in Eq. (22) describes the potential scattering of an electron with initial momentum $\boldsymbol{k}_i$ on a local potential $V(\boldsymbol{r})$, so that the electron momentum after the scattering is $\boldsymbol{k}_s$ and that L photons are exchanged with the laser field. It is given by Eq. (11), where $J_L(x)$ is the ordinary Bessel function of order L, $x = (A_0/\omega)\hat{\mathbf{e}}\cdot(\boldsymbol{k}_i - \boldsymbol{k}_s)$, and $V_{\boldsymbol{k}_i - \boldsymbol{k}_s}$ is the Fourier transform of the scattering potential $V(\boldsymbol{r})$. The differential cross section $d\sigma_{fs}(N,\Omega_s,\Omega_f)$ in Eq. (22) describes the subsequent potential scattering of the same electron with momentum $\boldsymbol{k}_s$ on a local potential $V(\boldsymbol{r})$, so that the electron momentum after the scattering is $\boldsymbol{k}_f$ and that N photons are exchanged with the laser field. It is given again by Eq. (11). Inserting Eq. (11) into Eq. (22), we obtain

$$d\sigma^{\mathrm{DS}}_{fi}(M,\Omega_f) = \rho(2\pi)^8 \frac{k_f}{k_i} \sum_L \int_0^{2\pi} d\phi_s \int_0^{\pi} d\theta_s \sin\theta_s J_L^2(x) \times |V_{\boldsymbol{k}_i - \boldsymbol{k}_s}|^2 J_N^2(y) |V_{\boldsymbol{k}_s - \boldsymbol{k}_f}|^2, \tag{23}$$

where $y = (A_0/\omega)\hat{\mathbf{e}}\cdot(\boldsymbol{k}_s - \boldsymbol{k}_f)$.

We model the scattering potential by the double Yukawa potential [42],

$$V(r) = -\frac{Z}{H}\frac{e^{-r/D}}{r}[1 + (H-1)e^{-Hr/D}], \tag{24}$$

where Z is the nuclear charge, D is the fitting parameter of the double Yukawa potential, and $H = DZ^{0.4}$. Values of D for different atoms are given in [43]. For the He atom, $Z=2$ and $D=0.215$. The Fourier transform of the potential (24) is

$$V_{\boldsymbol{P}} = -\frac{Z}{2\pi^2 H}\left[\frac{1}{\boldsymbol{P}^2 + \lambda_1^2} + \frac{H-1}{\boldsymbol{P}^2 + \lambda_2^2}\right], \tag{25}$$

where $\lambda_1 = 1/D$ and $\lambda_2 = (H+1)/D$. In our case, $\boldsymbol{P} = \boldsymbol{k}_i - \boldsymbol{k}_s$ for the first scattering and $\boldsymbol{P} = \boldsymbol{k}_s - \boldsymbol{k}_f$ for the second one.

We assumed that the laser-field polarization vector $\hat{\mathbf{e}}$ and the incident electron momentum $\boldsymbol{k}_i$ are in the direction of the polar axis, so that $J_L(x)$, $J_N(y)$, and $V_{\boldsymbol{k}_i - \boldsymbol{k}_s}$ in Eq. (23) are independent of the polar angle ϕ_s. The only term on the right-hand side of Eq. (23) that depends on the polar angle ϕ_s is $|V_{\boldsymbol{k}_s - \boldsymbol{k}_f}|^2$. We show elsewhere [44] that the integral $\int_0^{2\pi} d\phi_s |V_{\boldsymbol{k}_s - \boldsymbol{k}_f}|^2$ is independent of the polar angle ϕ_f, so that $d\sigma^{\mathrm{DS}}_{fi}(M,\Omega_f) = d\sigma^{\mathrm{DS}}_{fi}(M,\theta_f)$.

B. Energy-conserving conditions and the cutoff energy

The double scattering is an incoherent process and we have two energy-conserving conditions. The energy-conserving condition for the first scattering is $E_s = E_i + L\omega$, where $E_i = k_i^2/2$ is the incident electron energy and $E_s = k_s^2/2$ is the electron energy after the first scattering. The energy-conserving condition for the second scattering is $E_f = E_s + N\omega$, where $E_f = k_f^2/2$ is the final electron energy (after the second scattering). Combining these two conditions, we have $E_f = E_i + M\omega$, with $M = N+L$ the total number of absorbed (emitted) laser photons.

As we have already mentioned, the differential cross section for the direct (single) scattering, presented as a function of the final electron energy, forms a plateau structure with an abrupt cutoff at some boundary value of energy. Furthermore, there are two plateaus and two cutoffs in the case of rescattering [11,12]. Thus, we expect a cutoff-like behavior

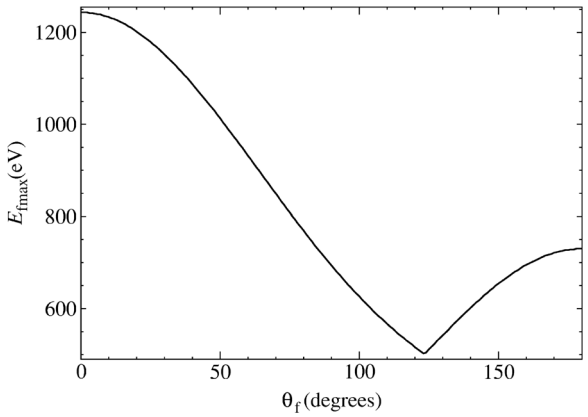

FIG. 2. Classical results for the maximum value of the final electron energy in the double scattering process as a function of the final electron scattering angle θ_f. The laser wavelength is 850 nm and the intensity 4.5×10^{14} W/cm^2. The kinetic energy of the incident electrons is E_i=17 eV and the geometry $\hat{\mathbf{e}}=\hat{\boldsymbol{k}}_i$ is assumed.

of the double-scattering spectra. The method of the steepest descent (stationary phase method) provides two semiclassical equations in the case of the double scattering. These equations are

$$[\boldsymbol{k}_i+\boldsymbol{A}(t_1)]^2=[\boldsymbol{k}_s+\boldsymbol{A}(t_1)]^2,\quad [\boldsymbol{k}_s+\boldsymbol{A}(t_2)]^2=[\boldsymbol{k}_f+\boldsymbol{A}(t_2)]^2, \tag{26}$$

with t_1 and t_2 the times of the first and the second scattering, respectively. The first of Eqs. (26) gives a quadratic equation for k_s, while the second one gives a quadratic equation for k_f. Combining the solutions k_s and k_f of these quadratic equations and performing numerical calculations, we can find the maximum value of the final electron energy, i.e., the cutoff energy. This is illustrated in Fig. 2, where the maximum value of the final electron energy is presented as a function of the final electron scattering angle θ_f. We see that the cutoff energy of the double scattering has the highest value for $\theta_f=0^\circ$.

The value of the cutoff energy for double scattering can be estimated similarly as was done for the ISLAR process. The first equation in Eqs. (26), for a linearly polarized monochromatic laser field and backward scattering ($\theta_s=180^\circ$; see the solid curve in the lower right panel of Fig. 8), gives $N_{\max}\omega=8U_P(1+\gamma_i)$, where γ_i was defined below Eq. (21) (see also Eq. (31) in the first reference in [12]), and $k_{s,\max}=2A_0+k_i$. Introducing this into the second equation in Eqs. (26), we obtain that $k_{f,\max}=4A_0+k_i$ for $\theta_f=0^\circ$. This leads to $L_{\max}\omega=8U_P(3+\gamma_i)$, so that

$$E_{f,\max}=E_i+(N_{\max}+L_{\max})\omega=E_i+16U_P(2+\gamma_i). \tag{27}$$

V. NUMERICAL RESULTS FOR THE FOCAL-AVERAGED SPECTRA

For all numerical examples presented in this section we will suppose that the laser field is monochromatic and linearly polarized, with the electric field given by Eq. (4) and the polarization vector $\hat{\mathbf{e}}$ in the direction of the polar axis. In the case of laser-assisted electron-ion radiative recombination (LAR, SLAR, and ISLAR), the polarization vector $\hat{\mathbf{e}}_{\boldsymbol{K}}$ of the emitted x rays is parallel and the incident electron momentum $\boldsymbol{k}_i$ is antiparallel to the laser-field polarization vector ($\hat{\mathbf{e}}=\hat{\mathbf{e}}_{\boldsymbol{K}}=-\hat{\boldsymbol{k}}_i$; see Fig. 1). For the electron-atom scattering and the double scattering, the incident electron momentum is parallel to the laser-field polarization vector ($\hat{\mathbf{e}}=\hat{\boldsymbol{k}}_i$).

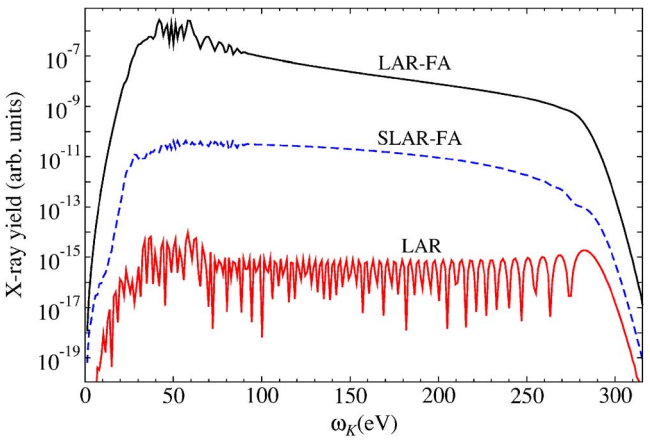

FIG. 3. (Color online) The focal-averaged x-ray energy spectra for the laser-assisted radiative recombination of electrons with He^+ ions. The incident electron kinetic energy is E_i=25 eV. The laser field is monochromatic and linearly polarized, with a wavelength of 1064 nm and a maximum intensity $I_{\max}=6\times10^{14}$ W/cm^2. The polarization vectors of the laser field and the x-ray field are in the direction of the polar axis, with the incident electron momentum in the opposite direction ($\hat{\mathbf{e}}=\hat{\mathbf{e}}_{\boldsymbol{K}}=-\hat{\boldsymbol{k}}_i$). The focal-averaged results for LAR (solid black line, denoted by LAR-FA) and SLAR (dashed blue line, denoted by SLAR-FA) are presented, as well as the scaled differential power spectrum for LAR with fixed intensity $I=I_{\max}$ (solid red line, denoted by LAR).

A. X-ray energy spectra

In Fig. 3 we present the focal-averaged x-ray energy spectra for the laser-assisted radiative recombination of electrons with He^+ ions. The kinetic energy of the incident electrons is E_i=25 eV. The laser wavelength is 1064 nm (Nd:YAG laser) and the intensity is 6×10^{14} W/cm^2. A detailed analysis of the laser-assisted electron-ion radiative recombination, for a fixed laser-field intensity, is given in Ref. [4], where the S-matrix theory in the second Born approximation was applied. The S matrix (as well as the T matrix derived from it) consists of the two terms: the first term describes the direct electron-ion radiative recombination (LAR), while the second term describes the electron-ion radiative recombination with a previous electron scattering on the same ion (SLAR). Since the differential power spectrum for electron-ion radiative recombination is proportional to the absolute square of the T matrix, it depends on the coherent sum of these two terms. Therefore, if both terms are taken into account, the final result will include both the LAR and SLAR processes. In our example presented in Fig. 3, the focal-averaged results for LAR and SLAR are calculated separately (but in the same arbitrary units) and we can see that the contribution of

LAR is dominant. Thus, the inclusion of the second term in the T matrix does not affect the final result significantly [45].

In Fig. 3, the differential power spectrum of LAR for fixed intensity $I=I_{max}$ is also presented. The ordinate of the differential power spectrum (in atomic units) as a function of the x-ray energy is shifted down by six orders of magnitude for a better visual comparison with the focal-averaged yields. One can see that the LAR result for fixed intensity has a rather flat plateau, while the focal-averaged results exhibit an inclined plateau in which the yield decreases with the increase of the x-ray photon energy. The explanation is the following: The cutoff energy of the emitted x rays decreases with the decrease of the laser-field intensity. On the other hand, the focal-averaging procedure includes the summation over all intensities between $I=0$ and $I=I_{max}$. Therefore, with the increase of the emitted x-ray energy, less and less intensities in the sum give a contribution to the total yield, the lower intensities being gradually eliminated.

One can also see that the oscillations in the middle- and high-energy part of the spectrum are absent for the focal-averaged results. The LAR spectrum for fixed intensity exhibits a lot of oscillations. This can be explained using semiclassical analysis [3,4]. Four saddle-point solutions contribute to the low-energy part of the spectrum. Their interference is responsible for a complicated oscillatory behavior of the low-energy part of the spectrum. However, only two saddle-point solutions contribute to the high-energy part of the spectrum, so that the corresponding oscillations are more regular. This also explains why the oscillations in the high-energy part of the spectrum are absent for the focal-averaged results. Namely, the energy value at which the transition from the two-saddle-point-solution regime to the regime with four saddle-point solutions occurs becomes lower with the decrease of the laser-field intensity. As a consequence, the more complicated interference structures in the non-averaged result shift to the left part of the energy spectrum (toward the lower energies) with the decrease of the laser-field intensity. Analogously, the oscillations in the focal-averaged spectrum shift toward the lower energies as the maximum value of the laser-field intensity decreases.

B. Scattered electron spectra

Figure 4 shows the focal-averaged spectrum (solid line) for laser-assisted potential scattering of electrons on He atoms as a function of the number of photons, n, exchanged with the laser field. The incident electron kinetic energy is $E_i=11$ eV and the scattering angle is $\theta_f=0^\circ$. The laser wavelength and maximum intensity are 1064 nm and $I_{max}=2.4\times10^{14}$ W/cm^2, respectively. The focal-averaged spectrum is compared with the spectrum for fixed intensity $I=I_{max}$ (dashed line). The ordinate of the differential cross section for fixed intensity as a function of the number of exchanged photons is in units (10^6 a.u.).

A detailed analysis of the laser-assisted electron-atom potential scattering was presented in Ref. [12], where the S-matrix theory in the second Born approximation with respect to the scattering potential has been applied, while the influence of the laser field was taken into account exactly through the Volkov states. The differential cross section was calculated by taking into account the first two terms of the T-matrix expansion. The first term is responsible for the direct electron-atom scattering, while the second term describes the rescattering (scattering with a repeated scattering on the same atom). Thus, the differential cross section includes both the direct scattering and the rescattering. Our present calculation is also performed in the second Born approximation, so that the focal-averaged spectrum and the result for fixed intensity, presented in Fig. 4, include both of the mentioned processes. Looking at the focal-averaged electron yield, one can notice two decreasing plateaus. The first plateau is a consequence of the direct scattering, while the second plateau is due to rescattering. The cutoff of the first plateau is at $n=93$, while the second plateau has a cutoff at $n=205$. These cutoff values are obtained by a classical analysis (see Ref. [12]). The spectrum for fixed intensity has the same cutoff values, but the plateaus are flat and with characteristic oscillations. Analogously to the LAR process, these oscillations are a consequence of the interfering semiclassical solutions of the saddle-point equations. The oscillations are suppressed and the plateaus become inclined if the focal averaging is applied, as one can see from Fig. 4.

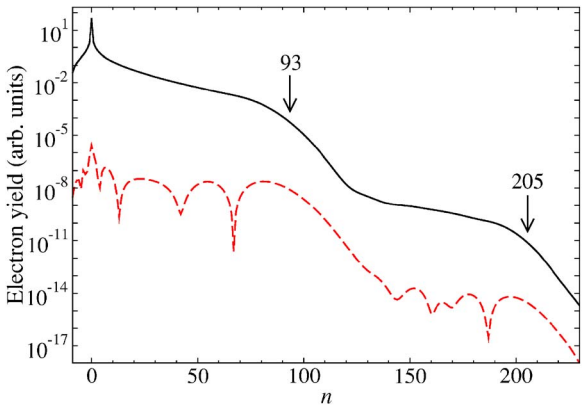

FIG. 4. (Color online) The focal-averaged spectrum (electron yield presented by the solid line) for potential scattering of electrons on He atoms in the presence of a monochromatic linearly polarized laser field, presented as a function of the number of photons, n, exchanged with the laser field. The laser wavelength is 1064 nm and the maximum intensity $I_{max}=2.4\times10^{14}$ W/cm^2. The kinetic energy of incident electrons is $E_i=11$ eV and the scattering angle is $\theta_f=0^\circ$. The polarization vector of the laser field and the incident electron momentum are in the direction of the polar axis ($\hat{\mathbf{e}}=\hat{\boldsymbol{k}}_i$). The scaled differential scattering cross section as a function of the number of exchanged photons, for the fixed intensity $I=I_{max}$, is presented by the dashed line.

The influence of the electron scattering angle on the focal-averaged spectra is analyzed in Fig. 5. The kinetic energy of incident electron and the laser-field parameters are the same as in Fig. 4. From Fig. 4 and the top left panel of Fig. 5, one can see that both plateaus become shorter with the increase of the scattering angle θ_f. As θ_f increases toward a boundary value ($\theta_f=32^\circ$ for the parameters of Fig. 5), the cutoff position of the first plateau shifts more and more rapidly to the left side of the spectrum. The first plateau practically vanishes when this boundary value is reached. With a further

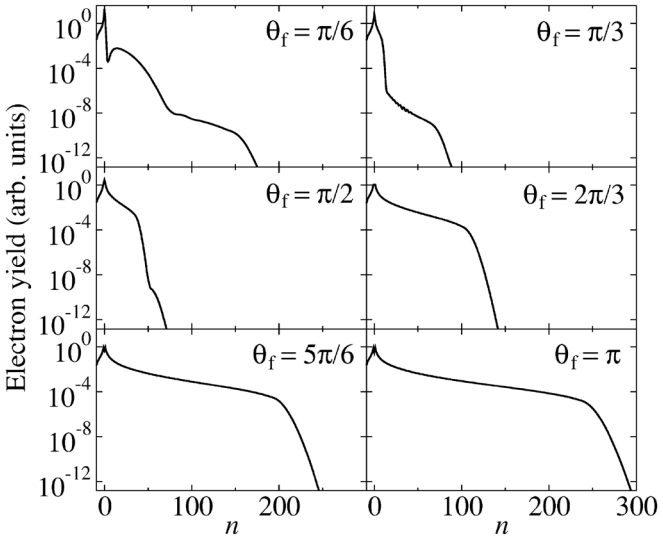

FIG. 5. The focal-averaged spectra for potential scattering of electrons on He atoms in the presence of a monochromatic linearly polarized laser field, presented as functions of the number of photons, n, exchanged with the laser field. The kinetic energy of the incident electrons and the laser-field parameters are the same as in Fig. 4. The geometry $\hat{\mathbf{e}}=\hat{\boldsymbol{k}}_i$ is assumed and the scattering angle θ_f is denoted in each panel. The same arbitrary units are employed in each panel.

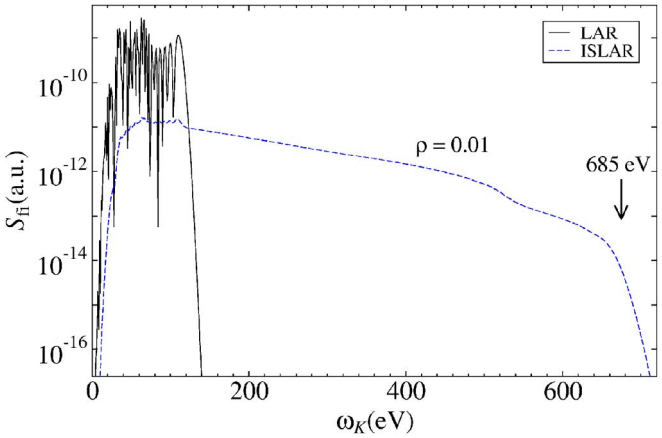

FIG. 6. (Color online) The differential power spectra as functions of the emitted x-ray energy, for the electron–He^+-ion radiative recombination, in the presence of a monochromatic linearly polarized laser field having a wavelength 1064 nm and an intensity 3.1×10^{14} W/cm^2, and for incident electron energy E_i=2 eV. The geometry $\hat{\mathbf{e}}=\hat{\mathbf{e}}_K=-\hat{\boldsymbol{k}}_i$ is assumed. The ion beam density and thickness are such that the parameter ρ=0.01 a.u. The results for LAR (solid line) and ISLAR (dashed line) are presented. The cutoff value of the x-ray energy for the ISLAR process is denoted.

increase of the angle θ_f, the first plateau appears again and becomes wider. The cutoff position shifts slowly to the right-hand side of the spectrum (see the panels with $\theta_f \geqslant \pi/3$ in Fig. 5). While the length of the first plateau increases with the increase of θ_f above the boundary value θ_f=32°, the second plateau is becoming shorter and shorter. For large values of θ_f, the cutoff value of the first plateau is larger than that of the second plateau (for a better insight, see Fig. 7 in the first of Ref. [12]). In this case, the first plateau masks the second and the rescattering contribution is not visible anymore (see the panels with $\theta_f \geqslant 2\pi/3$ in Fig. 5). These results are confirmed by the classical analysis presented in Ref. [12]. Qualitatively similar results can be obtained without the focal averaging (i.e., with a fixed intensity). Comparison of such spectra with those of Fig. 5 shows that the plateaus are more inclined and that the interference oscillations are suppressed for the focal-averaged spectra. The effect of focal averaging is similar to that presented in Fig. 4.

VI. NUMERICAL RESULTS FOR INCOHERENT PROCESSES

We now turn our attention to the incoherent processes in order to compare them with the corresponding coherent processes. In the following examples, we assume that the parameter ρ takes the value ρ=0.01 a.u. Since the differential power spectrum of the ISLAR process, Eq. (5), and the differential cross section for double scattering, Eq. (22), are directly proportional to ρ, the results presented below can easily be adjusted to different values of ρ by shifting the corresponding curves up or down by the factor ρ. In Ref. [26] it was estimated that, in the case of double scattering, ρ=0.03 a.u. for He and ρ=0.015 a.u. for Ar. The estimate of the value of ρ was based on observation of double-scattering effects in the excitation of the 2 ^1P level of He.

In Fig. 6, the differential power spectra of LAR (solid line) and ISLAR (dashed line) are presented as functions of the emitted x-ray energy for a recombination of electrons having energy E_i=2 eV with He^+ ions in the presence of a Nd:YAG laser of intensity 3.1×10^{14} W/cm^2. One can notice that the cutoff energy of the ISLAR process is much higher than that of the LAR process. Equation (21), taking into account that $|E_B|$=24.59 eV for He, gives $\omega^{\mathrm{IS}}_{\boldsymbol{K},\max}$=685 eV, which agrees very well with the result presented in Fig. 6. On the other hand, according to Eq. (20), the cutoff energy for the LAR process is 115 eV, i.e., the plateau is six times shorter than that of the ISLAR process.

Let us now compare the double electron-atom potential scattering with the electron-atom potential scattering in the second Born approximation (2B). In both cases, we model the scattering potential by the double Yukawa potential, Eq. (24). In Fig. 7, the differential cross sections for laser-assisted potential scattering of electrons on He atoms are presented as functions of the final electron energy. The laser wavelength is 850 nm and the intensity is 4.5×10^{14} W/cm^2. The kinetic energy of the incident electrons is E_i=17 eV and the scattering angle of the final-state electrons is θ_f=0°. The results for scattering in the second Born approximation (solid line, denoted by 2B) and for double scattering (dashed line, denoted by DS) are presented. The cutoff energy for double scattering is much higher than the cutoff energies for the direct scattering and rescattering (the 2B curve includes both the direct scattering and the rescattering), as one can see from Fig. 7. Equation (27), for the parameters of Fig. 7, gives $E_{f,\max}$=1245 eV, which agrees very well with the numerical results presented in Figs. 2 and 7.

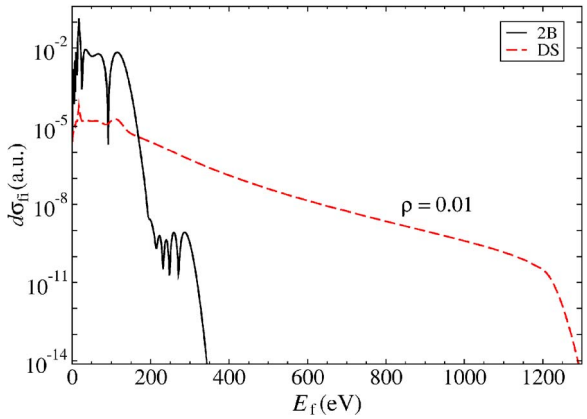

FIG. 7. (Color online) The differential cross sections for potential scattering of electrons on He atoms in the presence of a monochromatic linearly polarized laser field, as functions of the final electron energy. The laser wavelength is 850 nm and the intensity 4.5×10^{14} W/cm^2. The kinetic energy of the incident electrons is E_i=17 eV, the scattering angle of the final-state electrons is θ_f=0°, and the geometry $\hat{\mathbf{e}}=\hat{\mathbf{k}}_i$ is assumed. The atomic beam density and thickness are such that the parameter ρ=0.01 a.u. The results for the coherent scattering in the second Born approximation (solid line, denoted by 2B) and for the incoherent double scattering (dashed line, denoted by DS) are presented.

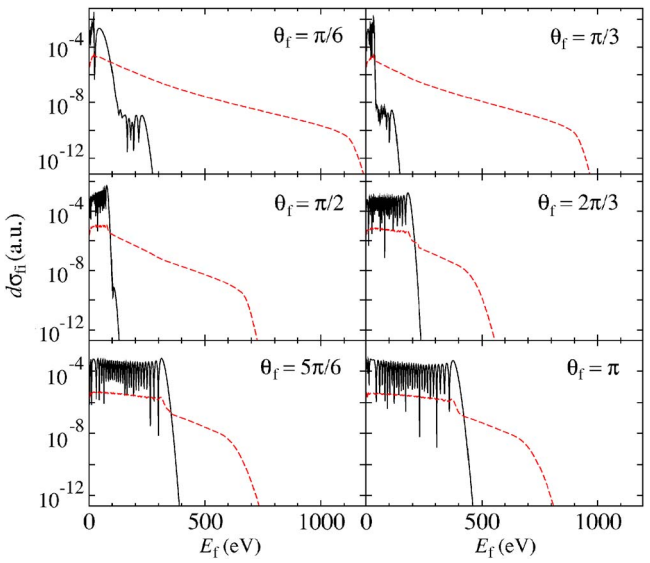

FIG. 8. (Color online) The differential cross sections for laser-assisted potential scattering of electrons on He atoms as functions of the final electron energy. The incident electron, laser field, and atomic beam parameters are the same as in Fig. 7. The scattering angle θ_f of the final-state electrons is denoted in each panel. The results for the coherent scattering in the second Born approximation (solid lines) and for the incoherent double scattering (dashed lines) are presented.

The influence of the final-electron scattering angle on the double scattering spectra is analyzed in Fig. 8. The other parameters are as in Fig. 7. In each panel of Fig. 8, the results for scattering in the second Born approximation (solid line) and for the double scattering (dashed line) are compared. The results for double scattering are in accordance with the dependence of the cutoff energy on the scattering angle θ_f (see Sec. IV B and Fig. 2).

VII. CONCLUSIONS

We have shown that the focal-averaged spectra of the x rays emitted in the laser-assisted radiative recombination and the focal-averaged spectra of the scattered electrons in the laser-assisted electron-atom potential scattering are qualitatively similar to those obtained with a fixed laser-field intensity. The difference is that the plateaus of the focal-averaged spectra are more inclined and that the oscillatory structure of these spectra is either absent or suppressed, while the spectra for fixed intensity have rather flat plateaus with the pronounced interference oscillations. The structure of the focal-averaged spectra is explained using semiclassical results for the laser-field-intensity dependence of the cutoff of the x-ray and electron energy spectra, as well as the dependence of the number of interfering saddle-point solutions on the laser-field intensity.

Further, we have shown that the incoherent processes (the processes that include incoherent scattering), such as ISLAR and double scattering, exhibit a plateaulike structure with much longer plateaus than those of the corresponding coherent processes. The cutoff positions of these incoherent-scattering-induced plateaus are explained using semiclassical arguments, both for ISLAR and for double scattering. In particular, a simple analytical formula (21) for the maximum energy of the x rays emitted in the ISLAR process is derived. For high laser-field intensities, this energy is nine times higher than the corresponding energy of the LAR process [compare Eqs. (20) and (21) for a high ponderomotive energy]. The contributions (i.e., the plateau heights) of the incoherent processes may be considerable, provided the atomic (ionic) beam density is high and/or its diameter is large.

ACKNOWLEDGMENTS

We gratefully acknowledge support by the Volkswagen-Stiftung, by the Ministry of Education and Science, Canton Sarajevo, and by the Federal Ministry of Education and Science, Bosnia and Herzegovina.

[1] D. B. Milošević and F. Ehlotzky, Adv. At., Mol., Opt. Phys. **49**, 373 (2003).

[2] A. Jaroń, J. Z. Kamiński, and F. Ehlotzky, Phys. Rev. A **61**, 023404 (2000); **63**, 055401 (2001); Laser Phys. **11**, 174 (2001); J. Phys. B **34**, 1221 (2001); J. Z. Kamiński and F. Ehlotzky, Opt. Commun. **234**, 343 (2004).

[3] M. Yu. Kuchiev and V. N. Ostrovsky, Phys. Rev. A **61**, 033414 (2000); J. Phys. B **34**, 405 (2001).

[4] D. B. Milošević and F. Ehlotzky, Phys. Rev. A **65**, 042504 (2002); J. Mod. Opt. **50**, 657 (2003).
[5] C. Leone, S. Bivona, R. Burlon, and G. Ferrante, Phys. Rev. A **66**, 051403(R) (2002); S. Bivona, R. Burlon, G. Ferrante, and C. Leone, Laser Phys. Lett. **1**, 86 (2004); **1**, 118 (2004); Appl. Phys. B **78**, 809 (2004); J. Opt. Soc. Am. B **22**, 2076 (2005).
[6] T. Cheng, X. Li, S. Ao, L.-A. Wu, and P. Fu, Phys. Rev. A **68**, 033411 (2003).
[7] S. X. Hu and L. A. Collins, Phys. Rev. A **70**, 013407 (2004); **70**, 035401 (2004).
[8] J. Z. Kamiński and F. Ehlotzky, Phys. Rev. A **71**, 043402 (2005); J. Mod. Opt. **53**, 7 (2006).
[9] S. Bivona, R. Burlon, G. Ferrante, and C. Leone, Opt. Express **14**, 3715 (2006).
[10] F. Ehlotzky, A. Jaroń, and J. Z. Kamiński, Phys. Rep. **297**, 63 (1998).
[11] N. L. Manakov, A. F. Starace, A. V. Flegel, and M. V. Frolov, Pis'ma Zh. Eksp. Teor. Fiz. **76**, 316 (2002) [JETP Lett. **76**, 258 (2002)]; Phys. Lett. A **334**, 197 (2005); M. V. Frolov, A. V. Flegel, N. L. Manakov, and A. F. Starace, J. Phys. B **38**, L375 (2005).
[12] A. Čerkić and D. B. Milošević, Phys. Rev. A **70**, 053402 (2004); Laser Phys. **15**, 268 (2005); Phys. Rev. A **73**, 033413 (2006).
[13] H.-J. Kull, J. Görlinger, and L. Plagne, Laser Phys. **10**, 151 (2000); J. Görlinger, H.-J. Kull, and V. T. Tikhonchuk, *ibid.* **15**, 245 (2005); H.-J. Kull and V. T. Tikhonchuk, Phys. Plasmas **12**, 063301 (2005).
[14] D. B. Milošević and F. Ehlotzky, Phys. Rev. A **58**, 2319 (1998).
[15] D. B. Milošević and A. F. Starace, Phys. Rev. Lett. **81**, 5097 (1998); J. Phys. B **32**, 1831 (1999); Phys. Rev. A **60**, 3943 (1999); Laser Phys. **10**, 278 (2000).
[16] D. B. Milošević, D. Bauer, and W. Becker, J. Mod. Opt. **53**, 125 (2006).
[17] We will use atomic units ($e=\hbar=m_e=4\pi\varepsilon_0=1$).
[18] J. H. Eberly, J. Javanainen, and K. Rzążewski, Phys. Rep. **204**, 331 (1991).
[19] W. Becker, F. Grasbon, R. Kopold, D. B. Milošević, G. G. Paulus, and H. Walther, Adv. At., Mol., Opt. Phys. **48**, 35 (2002).
[20] P. J. Curry and W. R. Newell, J. Phys. B **17**, 3353 (1984).
[21] S. Bivona, R. Burlon, R. Zangara, and G. Ferrante, J. Phys. B **18**, 3149 (1985).
[22] A. Weingartshofer, J. K. Holmes, J. Sabbagh, and S. L. Chin, J. Phys. B **16**, 1805 (1983).
[23] It should be mentioned that there are no laser-assisted electron-atom scattering measurements yet for such strong laser intensities for which the mentioned plateau structures appear. For a more recent experimental work, see B. Wallbank and J. K. Holmes, Can. J. Phys. **79**, 1237 (2001).
[24] R. Kopold, W. Becker, M. Kleber, and G. G. Paulus, J. Phys. B **35**, 217 (2002).
[25] For not too short laser pulses, which we consider in the present paper, one cannot distinguish the directions $\hat{e}$ and $-\hat{e}$. However, for few-cycle pulses this is not so and the results obtained in the recent stereo-ATI experiment were used to determine the carrier-envelope phase difference, a quantity that is important for attoscience: D. B. Milošević, G. G. Paulus, D. Bauer, and W. Becker, J. Phys. B **39**, R203 (2006).
[26] I. Rabadan, L. Mendez, and A. S. Dickinson, J. Phys. B **29**, L801 (1996).
[27] D. B. Milošević and F. Ehlotzky, J. Phys. B **30**, 2999 (1997).
[28] N. M. Kroll and K. M. Watson, Phys. Rev. A **8**, 804 (1973).
[29] D. B. Milošević, J. Phys. B **28**, 1869 (1995).
[30] B. Wallbank and J. K. Holmes, Phys. Rev. A **48**, R2515 (1993); J. Phys. B **27**, 1221 (1994); **27**, 5405 (1994).
[31] A. Weingartshofer, J. K. Holmes, G. Caudle, E. M. Clarke, and H. Kruger, Phys. Rev. Lett. **39**, 269 (1977).
[32] N. J. Mason and W. R. Nevell, J. Phys. B **20**, L323 (1987); N. J. Mason, Rep. Prog. Phys. **56**, 1275 (1993).
[33] C. Höhr, A. Dorn, B. Najjari, D. Fischer, C. D. Schröter, and J. Ullrich, Phys. Rev. Lett. **94**, 153201 (2005).
[34] T. W. Scott, Rev. Mod. Phys. **35**, 231 (1963).
[35] F. V. Bunkin and M. V. Fedorov, Zh. Eksp. Teor. Fiz. **49**, 1215 (1965) [Sov. Phys. JETP **22**, 844 (1965)].
[36] D. B. Milošević, Phys. Rev. A **53**, 619 (1996); L. W. Garland, A. Jaroń, J. Z. Kamiński, and R. M. Potvliege, J. Phys. B **35**, 2861 (2002).
[37] K. M. Dunseath and M. Terao-Dunseath, J. Phys. B **37**, 1305 (2004).
[38] D. B. Milošević, J. Phys. B **30**, 5251 (1997).
[39] B. Hüpper, J. Main, and G. Wunner, Phys. Rev. Lett. **74**, 2650 (1995); Phys. Rev. A **53**, 744 (1996).
[40] D. B. Milošević and F. Ehlotzky, Phys. Rev. A **58**, 3124 (1998); Laser Phys. **9**, 149 (1999).
[41] L. V. Keldysh, Zh. Eksp. Teor. Fiz. **47**, 1945 (1964) [Sov. Phys. JETP **20**, 1307 (1965)].
[42] A. E. S. Green, D. E. Rio, and T. Ueda, Phys. Rev. A **24**, 3010 (1981).
[43] A. E. S. Green, D. L. Sellin, and A. S. Zachor, Phys. Rev. **184**, 1 (1969).
[44] A. Čerkić and D. B. Milošević, J. Phys. B **39**, 4419 (2006).
[45] If we raise the laser-field intensity, the second plateau will appear in the SLAR results. This plateau will be much lower than the first one, but visible in the total LAR+SLAR result, since it appears in the high-energy region beyond the LAR cutoff [4]. However, the laser-field intensities of order 10^{15} W/cm^2 and above are required to obtain the second SLAR plateau.